Layered Black Phosphorus Nanoflakes Reduce Bacterial Burden and Enhance Healing of Murine Infected Wounds

Emmeline P. Virgo, Hanif Haidari, Zo L. Shaw, Louisa Z. Y. Huang, Tahlia L. Kennewell, Luke Smith, Taimur Ahmed, Saffron J. Bryant, Gordon S. Howarth, Sumeet Walia, Allison J. Cowin, Aaron Elbourne, and Zlatko Kopecki*

Current treatment modalities of cutaneous wound infections are largely ineffective, attributed to the increasing burden of antimicrobial resistance. *S. aureus*, a commonly wound-associated pathogen continues to pose a clinical challenge, suggesting that new alternative therapeutic materials are urgently required to provide optimal treatment. A layered allotrope of phosphorus termed Black Phosphorus nanoflakes (BPNFs) has emerged as a potential alternative antibacterial material. However, wider deployment of this material requires extensive biological validation using the latest pre-clinical models to understand its role in wound management. Here, the antibacterial potential of BPNFs against wound pathogens demonstrates over 99% killing efficiency at ambient conditions, while remaining non-toxic to mammalian skin cells. In addition, in vivo validation of BPNFs using a preclinical model of *S. aureus* acute wound infection demonstrates that daily topical application significantly reduces infection (3-log reduction) comparable to ciprofloxacin antibiotic control. Furthermore, the application of BPNFs also accelerates wound closure, increases wound re-epithelization, and reduces tissue inflammation compared to controls, suggesting a potential role in alleviating the current challenges of infected cutaneous wounds. For the first time, this study demonstrates the potential role of BPNFs in ambient light conditions for clearing a clinically relevant wound infection with favorable wound healing properties.

1. Introduction

The wound infection "epidemic" is becoming increasingly problematic, with antibiotic resistance mechanisms spreading widely and rapidly.[1] The impact of antimicrobial resistance has been predicted to result in excess of 10 million deaths by 2050, alongside significant clinical expenditure.[2] Currently, $\approx 70\%$ of bacteria have developed resistance to at least one common class of antibiotic, suggesting a desperate need for the development of new alternative antimicrobial therapeutics for clinical wound management.[3]

Clinical infection arises when wounds are colonized with invasive microorganisms, in particular gram-positive *Staphylococcus aureus (S. aureus)* which accounts for over 65% of chronic wound infections.[4] Multidrug-resistant *S. aureus*-induced infection is becoming a significant clinical challenge which increases the risk of patient morbidity and mortality.[5] *S. aureus* infected wounds are highly resistant to common therapeutics requiring prolonged treatment regimens and higher doses, which contribute to further bacterial resistance and host mammalian cell toxicity.[5]

E. P. Virgo, L. Smith, G. S. Howarth
School of Animal and Veterinary Sciences
The University of Adelaide
Roseworthy, SA 5371, Australia
E. P. Virgo, H. Haidari, T. L. Kennewell, L. Smith, A. J. Cowin, Z. Kopecki
Future Industries Institute
University of South Australia
Mawson Lakes, SA 5095, Australia
E-mail: zlatko.kopecki@unisa.edu.au

Z. L. Shaw, S. Walia
School of Engineering
STEM College
RMIT University
Melbourne, VIC 3001, Australia
L. Z. Y. Huang, S. J. Bryant, A. Elbourne
School of Science
STEM College
RMIT University
Melbourne, VIC 3001, Australia
T. Ahmed
Pak-Austria Fachhochschule
Institute of Applied Sciences and Technology
Haripur 22620, Pakistan

DOI: 10.1002/adtp.202300235

**ADVANCED
SCIENCE NEWS**

www.advancedsciencenews.com

**ADVANCED
THERAPEUTICS**

www.advtherap.com

The resulting infection complicates normal healing where antibiotic-resistant bacteria release adhesion, virulence, and antiphagocytic factors and induce neutrophil lysis, favoring further biofilm formation and ongoing inflammation.[5] The combination of these complications significantly increases the burden on patient well-being, hospital readmissions, healing outcomes, and overall healthcare costs.[6,7] Currently, available treatment options for antibiotic-resistant bacteria are becoming scarce, with poor antimicrobial stewardship and only five new classes of antibiotics discovered since 2000, highlighting the urgency to develop new alternative therapies to maintain gold-standard patient care.[1,8] Additionally, current wound dressings are commonly impregnated with antibiotics, antimicrobial agents, and growth factors and can create a sealed anaerobic environment, which favors mature biofilm formation and contributes to impaired wound healing.[9]

Nanotechnology involves materials sized within the nanoscale range of 1–100 nm.[10] Nanoparticles (NPs) have been successfully exploited in a wide range of biomedical industries including wound management.[11,12] Additionally, attractive customizable properties of NPs allow for a wide range of synthesis methods, including both metallic and non-metallic materials for the treatment of localized wound infection.[11] Among all, silver NPs (AgNPs) have been previously demonstrated as effective antimicrobial agents for both gram-negative and gram-positive organisms.[10] AgNP's antibacterial application is influenced by their physicochemical properties, release mechanism as well as delivery mode.[13,14] Although AgNPs are widely used in clinical wound management, the dressings have clear limitations including the lack of consistent antibacterial activity, low stability, high toxicity toward mammalian cells, and short therapeutic application time.[10,15,16] Therefore, current research is focused on the development of biocompatible, antimicrobial nanomaterials with synergistic wound healing-promoting properties for wider clinical application.

Black Phosphorus a 2D material has recently been identified as an attractive antimicrobial agent with potential roles in promoting key phases of wound healing.[17] The material's layered flake-like morphology often termed Black Phosphorus nanoflakes (BP-NFs) can be synthesized using many exfoliation techniques.[17] BPNFs are characterized by a distinct honeycomb lattice structure, with a pair of lone phosphorus atoms allowing for extreme air sensitivity.[18] BPNFs are composed of nanosheets that are held together in the vertical direction by weak van der Waals forces.[19,20] These unique structural features have previously permitted its application in electronic devices, however, the use of BPNFs in medical applications particularly as an antimicrobial agent has not been greatly explored to date. Indeed, no studies to date have investigated the role of BPNFs in wound applications, particularly wounds that are infected with drug-resistant pathogens.

BPNFs possess antimicrobial properties mediated by two major bacteria-killing mechanisms with unique nano-bio interface interactions.[21] The first mechanism is attributed to the physical characteristic of the nanoflake, known as the "nanoknife" effect where the sharp edges of the flake come into physical contact with the bacterial membrane triggering the damage and leakage of cytoplasmic content and subsequently bacterial death.[21] The second major antimicrobial mechanism arises from a photo-

oxidative reaction which produces singlet oxygen ($^1O_2$), hydroxyl (OH^-), and a superoxide (O_2^-) moiety, also known as reactive oxygen species (ROS).[19,22] Numerous studies to date have shown that ROS are produced through light-activated mechanisms, which is reflected in the use of near-infrared radiation (NIR) in all current in vivo studies with Black Phosphorous, compensating for the multi-layered structure.[18,23–29] Most of the current understanding of BP materials are associated with the use of nanohybrid combined with zinc oxide[30] or silver nanoparticles[24] or achieving synergistic effects through photothermal treatment.[27] Among them, a study has focused on BP-zinc oxide nanohybrid coated on a titanium surface to disinfect bacteria when activated with photothermal treatment, where they have demonstrated that 98% bacterial reduction can be achieved only when a high NIR light irradiation ($\lambda = 808$ nm; 5 min at 65°C) is used.[31] This not only presents low specificity, however, also the unwanted risk of in vivo toxicity, damage, and severe inflammation of tissue.[32] The current study for the first time reveals that layered BPNFs can mediate biological activity independent of NIR or similar light sources. Here, the ROS-mediated biological activity is induced under ambient light conditions offering flexibility, simplicity, and a wide range of application practicality **Scheme 1**.

In this study, we investigate the safety and efficacy of layered pristine-BPNFs using in vitro and in vivo preclinical infected murine wound models under ambient light conditions. The in vitro antibacterial activity of the developed BPNFs was tested against gram-positive and gram-negative bacteria, showing superior bacterial killing without causing any adverse effects on mammalian skin cells. Additionally, the efficacy of the developed BPNFs was tested using preclinical models of murine wound infection using *S. aureus* (Xen29) Scheme 1. This study showed promising potential in eliminating clinically relevant wound infections, while simultaneously promoting cutaneous wound healing as indicated by accelerated wound closure, re-epithelization, and a higher degree of neutrophils in the wound bed compared to both controls and industry standard. Excitingly, this study for the first time reveals that pristine BPNFs can perform independently of a light source to eliminate drug-resistant infection and promote the healing of clinically infected wounds, offering exciting avenues for future developments. In addition, the BPNFs can be synthesized at a scalable range with added flexibility to be integrated into wound dressings and formulations for topical applications.

2. Results and Discussion

2.1. Material Characterizations

BPNFs are allotropes of phosphorus that has an orthorhombic structure (**Figure 1**a) and their layers are held together by weak van der Waals forces.[33] The BPNFs solution was prepared using liquid-phase exfoliation in dimethyl sulfoxide (DMSO).[19,34] The BPNFs were characterized using a combination of spectroscopic and microscopic techniques following established protocols.[19,34] In the Raman spectrum (Figure 1b), three distinct peaks correspond to the signature BPNFs peaks, A^1_g (361 cm^{-1}), B^2_g (438 cm^{-1}), and A^2_g (465 cm^{-1}).[35,36] The flakes were visualized using transmission electron microscopy (TEM) showing a size of 850 nm (Figure 1c) which is closely supported by

ADVANCED
SCIENCE NEWS
www.advancedsciencenews.com

ADVANCED
THERAPEUTICS
www.advtherap.com
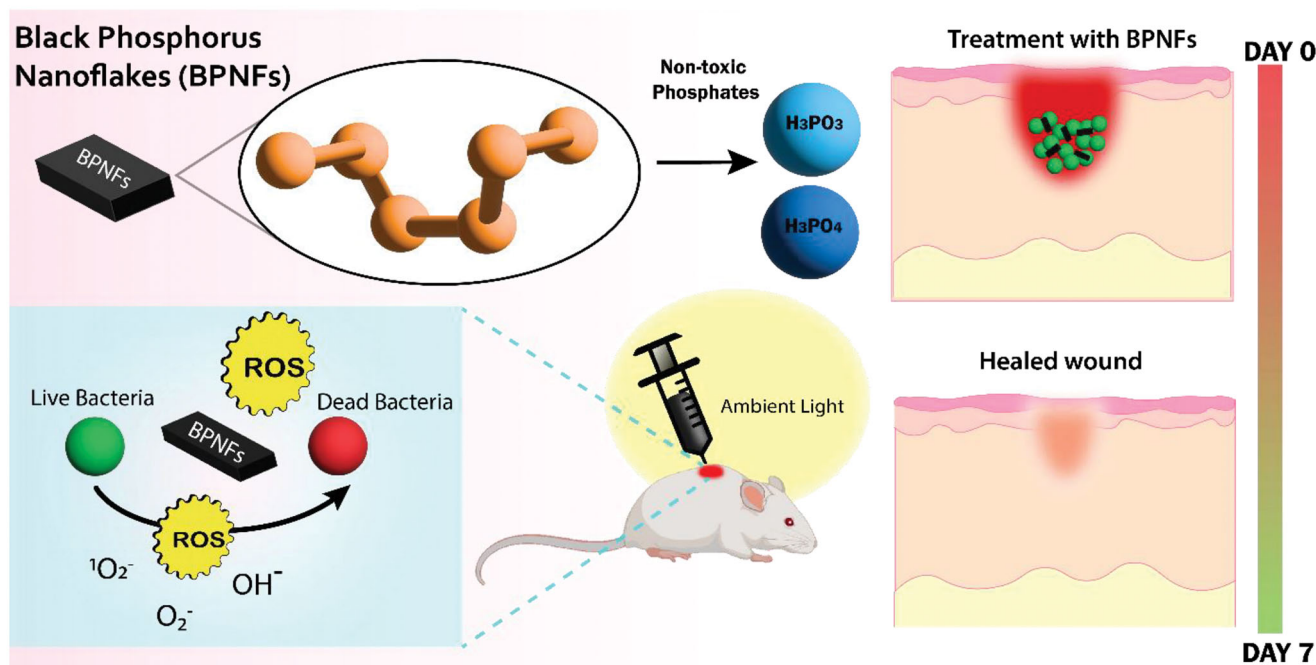
Scheme 1. Schematic illustration of BPNFs biological application and its role to eliminate wound infection while concurrently improving healing outcomes.

scanning electron microscopy (SEM) measurements of 900 nm flake size (Figure 1d). Further characterization was done using energy-dispersive X-ray spectroscopy (EDS) (Figure 1df). The EDS maps show the BPNFs are composed of primarily phosphorus atoms, with some oxygen atoms present. This oxygen can be attributed to the formation of an oxide layer.[37,38] The size distribution of the BPNFs was determined using atomic force microscopy (AFM) (Figure 1g). The average flake thickness was 41±33 nm (Figure 1h) and the average lateral size was 259±179 nm (Figure 1i). Additionally, further characterizations of selected bulk samples of different batches were measured to ensure consistency with the primary characterizations. The additional data of Raman spectra (Figure S1, Supporting Information), EDS Maps (Figure S2, Supporting Information), SEM (Figure S3, Supporting Information), TEM (Figure S4, Supporting Information) and AFM images (Figure S5, Supporting Information) of the BPNFs can be found in the supporting information, all showing similar functionality, morphology, and thickness which are consistent to Figure 1.

2.2. Cytotoxicity Evaluation

To optimize the concentration of BPNFs that was safe for use on mammalian skin cells, a dose-response experiment was performed. First, the cell viability was assessed using the Live/Dead assay by selecting low (1000 µg mL^{-1}) and high (1500 µg mL^{-1}) BPNFs concentrations. Fluorescent microscopy images confirmed that both treatment groups exhibited a high degree of green fluorescence and displayed normal HaCaTs and HFFs morphology comparable to the saline control (**Figure 2**a,b). Following quantification of bacterial viability, both human skin

cells demonstrated > 98% cell viability after 24 h of BPNFs treatment (Figure 2c), proposing a high degree of biocompatibility for clinical applications in wound management. These findings are in agreement with previously published studies, where the "nanoknife" effect had limited impact on mammalian cells, attributed to their difference in size compared to bacterial cells.[19] In addition, cell metabolic activity was determined following treatment in a dose-dependent manner using a resazurin assay. As shown in Figure 2d,e, concentrations of BPNFs < 1250 µg mL^{-1} demonstrated > 70% metabolic cell viability in both mammalian cell types suggesting a clinically acceptable level of active cell metabolism based on the industry standard of testing ISO 10993–5:2009, Biological Evaluation of in vitro cytotoxicity. However, BPNFs have the ability to absorb light at varying wavelengths, particularly between 550 and 590 nm (weak light absorption) and 250450 nm (strong light absorption).[39,40] Assessing cell viability using Live/Dead staining supported by microscopy images is the preferred way to measure cell viability and functionality for these kinds of materials. This minimizes light absorption during measurements providing more accurate measurements of their overall viability. Therefore, BPNFs at the optimal concentration can be used for topical wound application studies without negatively impacting mammalian skin cells.

2.3. In Vitro Antibacterial Activity of BPNFs

The antibacterial activity of the BPNFs at different concentrations was determined against gram-negative and gram-positive bacteria including *S. aureus (Xen 29 and MRSA)* and *S. epidermidis, P. aeruginosa,* and *E. coli*. These pathogens represent a high clinical relevance in the wound infection continuum. First, the

ADVANCED
SCIENCE NEWS

www.advancedsciencenews.com

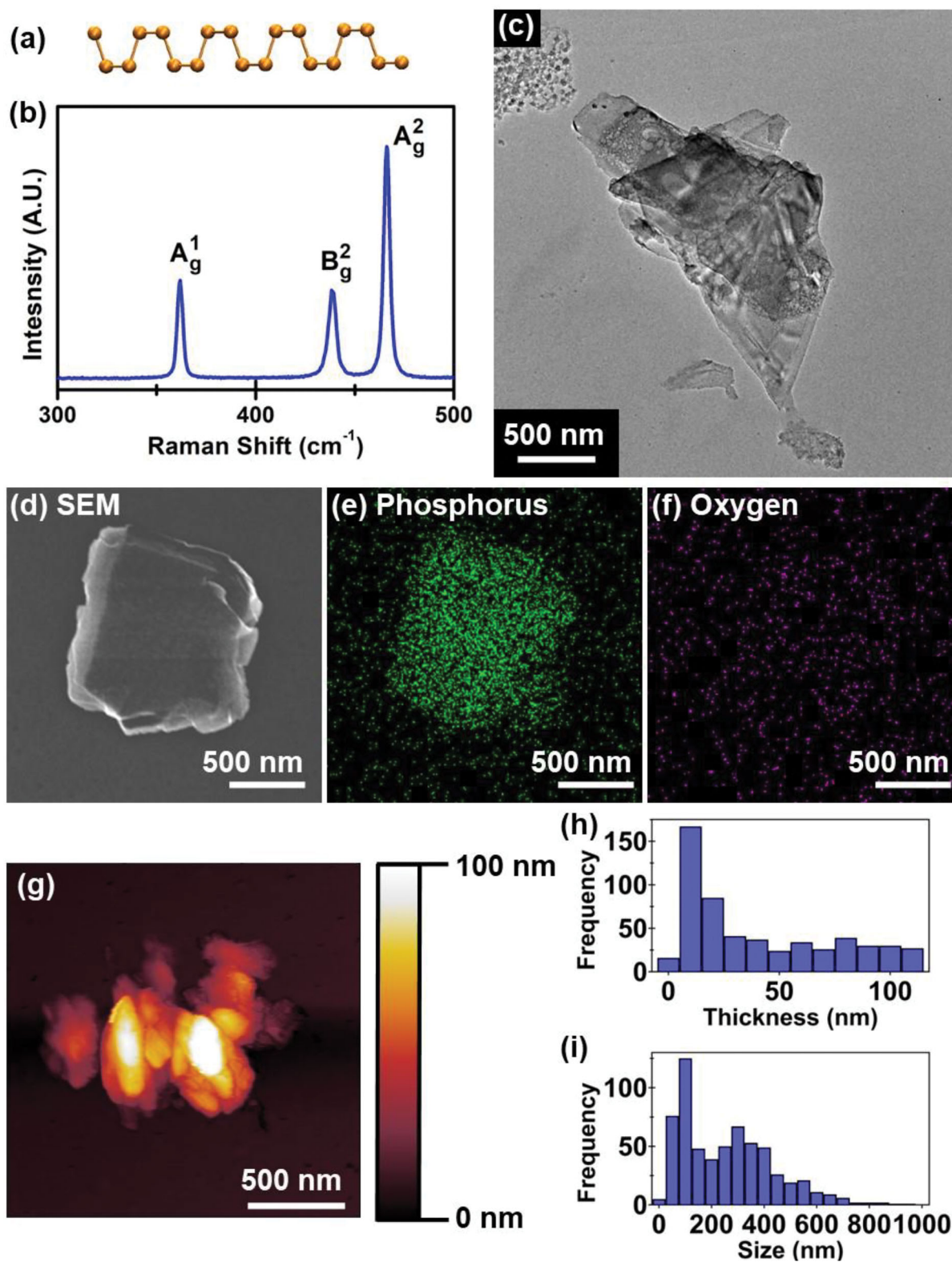**ADVANCED**
THERAPEUTICS

www.advtherap.com

Figure 1. Characterization of Black Phosphorus nanoflakes. a) Structure of pristine BPNFs. b) Raman spectra of exfoliated BPNFs deposited on a silicon substrate. c) TEM and d) SEM images of the BPNFs, and the corresponding EDS maps showing e) phosphorus and f) oxygen atoms. g) Representative AFM scan of a cluster of BPNFs used to determine the h) thickness and i) lateral size of the BPNFs in solution.
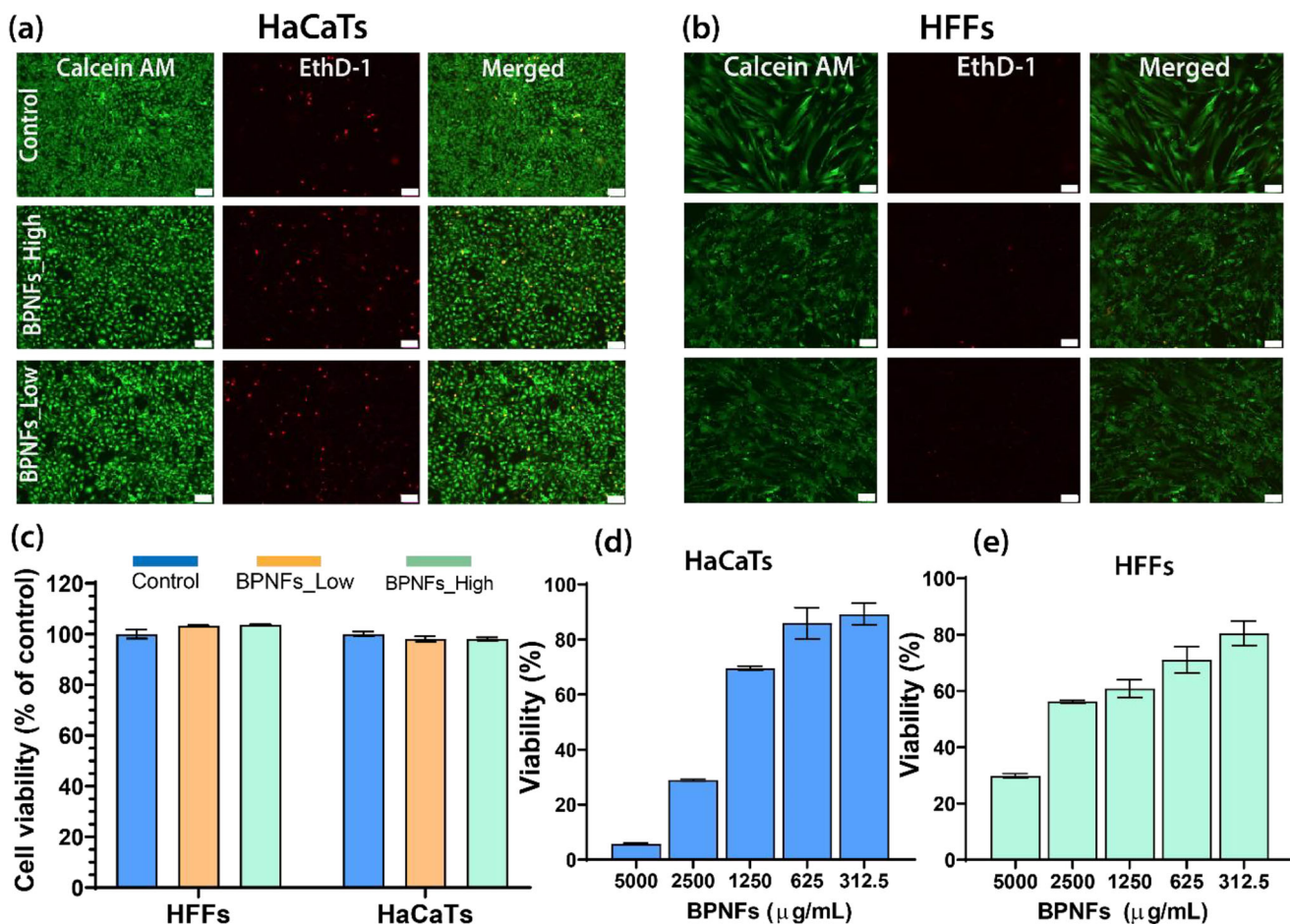
Figure 2. BPNFs had limited effects on skin cell viability. a,b) Representative images of HaCaTs and HFFs stained with Calcein AM (green) and dead cells stained with EthD-1 (red) following 24 h of treatment with BPNFs_Low (1000 µg ml^{-1}) and BPNFs_High (1500 µg ml^{-1}). c) The corresponding cell viability after treatment for both skin cells at low and high concentrations compared to control. d,e) In vitro metabolic skin cell activity was determined by a resazurin assay following 24 h of BPNFs treatment on HaCaTs and HFFs. Scale bar 50 µm. Data is shown as mean ± SEM.

minimum inhibitory concentration (MIC) of BPNFs against gram-negative and gram-positive pathogens was determined using a microdilution dose-response assay. This study demonstrates the antimicrobial properties of few-layered BPNFs through oxidation in ambient light conditions, without exposing the BPNFs sample to external light activation (i.e., NIR). Generally, BPNFs require activation energy to mediate their degradation causing ROS-mediated antibacterial killing. In this study, the BPNFs were found to have a MIC in the range of 750–1500 µg mL^{-1} in indoor laboratory light conditions. The MIC observed for *S. aureus* and *P. aeruginosa* was 1500 µg mL^{-1} while the MIC for *S. epidermidis* and *E. coli* was 750 µg mL^{-1} (Figure S1, Supporting Information). The effect of BPNFs on the MIC was also confirmed using a luminescent strain of *S. aureus* (Xen29) showed no detectable bacterial growth at 1500 µg mL^{-1} as denoted by the absence of luminescence in the wells (Figure S6, Supporting Information). The luminescent intensity was similar to that of sterile TSB confirming the near-complete inhibition of *S. aureus* treated with BPNFs at 1500 µg mL^{-1}. The antibacterial efficacy of most BPNFs is highly dependent on external light sources to activate the ROS mechanism to mediate the

antibacterial effect. We report an improved antibacterial activity against resistant bacteria, primarily due to BPNFs unique structural arrangement supported with controlled degradation in ambient light conditions.

Further, the time-dependent bacterial killing using gram-negative and gram-positive bacteria was also assessed using Live/Dead bacteria staining. Bacterial growth after each treatment was stained with a Live/Dead Baclight Viability kit (Thermo Fischer Scientific) and imaged using confocal microscopy. The kit contains SYT09/propidium iodide (PI) where the SYT09 stains intact membranes while the PI stains membranes that are compromised representing bright red fluorescence. The confocal images show distinct differences in the fluorescent intensity proportion between green/red. As shown in **Figure 3**ad, the control group for *S. aureus* and *P. aeruginosa* showed the highest green fluorescence indicating minimal cell death within 24 h resulting in over 95% cell viability. However, *S. aureus* treated with BPNFs showed a 62% loss of cell viability within 2 h, followed by an 80% loss of viability after 6 h (Figure 3a,b). After 24 h, over 99% of bacteria were killed as also indicated by the confocal images showing red and yellow fluorescence representing
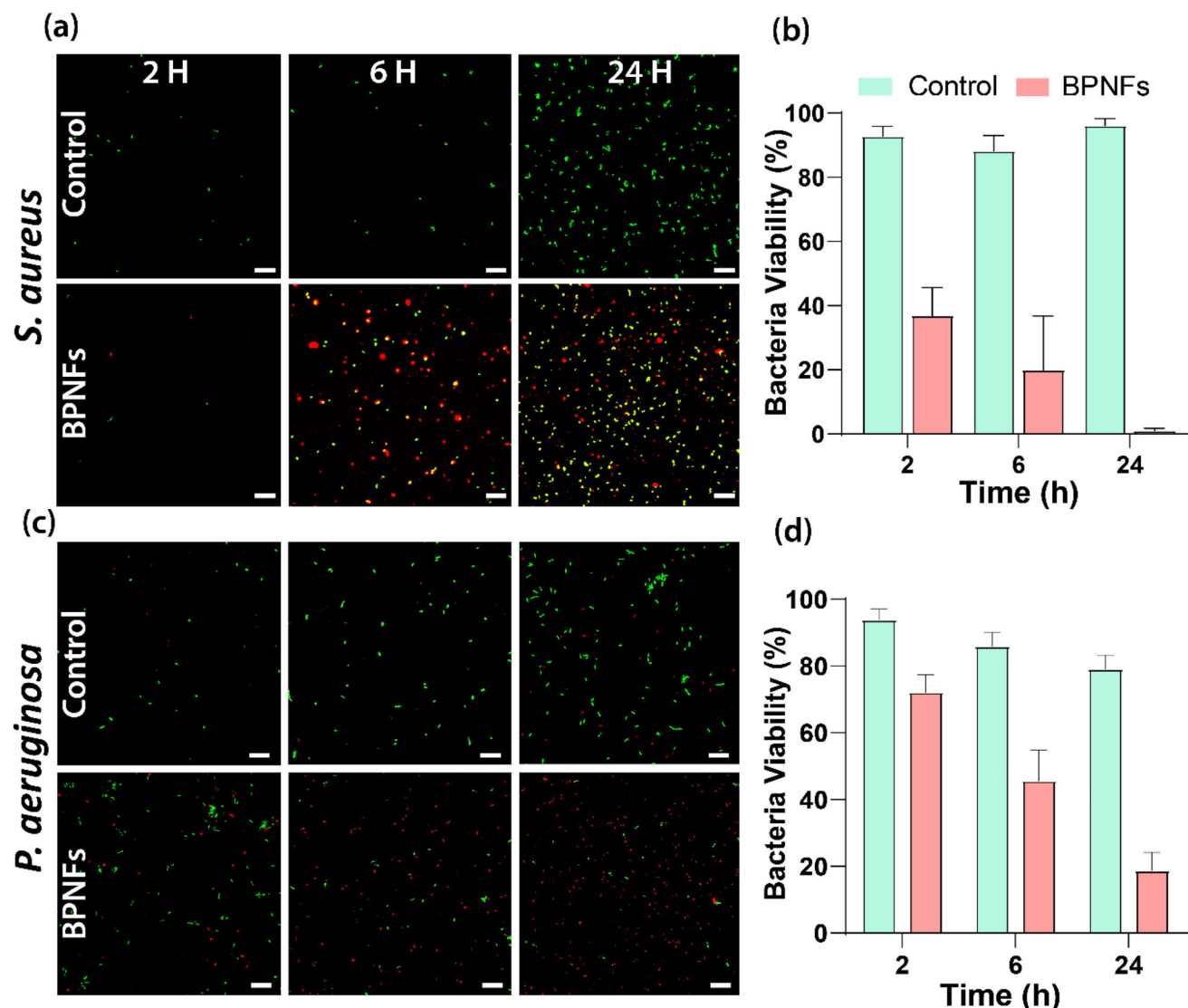
Figure 3. BPNFs in vitro antimicrobial effects against *S. aureus* and *P. aeruginosa*. a,b) Confocal images of time-dependent *S. aureus* and corresponding bacterial viability (%). c,d) Confocal images of *P. aeruginosa* and corresponding quantitative analysis of viability (%). Scale bar 10 µm. Data is shown as mean ± SD.

membrane-compromised cells. A similar trend was also observed in response to *P. aeruginosa* resulting in over 80% bacterial death after 24 h of treatment compared to the control (Figure 3d). This time-dependent killing assay supports the notion that the BPNFs could exert their antibacterial effect through physical contact, inducing membrane damage and rapid bacterial killing efficiency which could be highly useful for in vivo wound infection treatment to ensure rapid infection clearance.

2.4. In Vivo Antibacterial Effects of BPNFs

The in vivo antibacterial application of BPNFs was validated using a preclinical mouse wound infection model with daily treatment for 7 days. Once the *S. aureus* infection had developed, the mouse wounds were treated topically using either ciprofloxacin (antibiotic control), saline (negative control), or BPNFs (1500 µg mL^{-1}) daily. Following the Australian Code for the care and use of animals for scientific purposes, mice were housed in a controlled environment including an ambient light within limits compatible with rodent health and well-being including a 12h light/dark cycle as varied light/dark cycles require for regulation of rodent breeding and circadian rhythm. As shown in **Figure 4**a, there was a distinct difference in bacterial reduction as indicated by the photon intensity, where the antibiotic and BPNFs showed significantly decreased wound infection levels compared to the saline control (Figure 4a). Quantitative analysis of infection levels over time indicated that there was a consistent reduction in bacterial infection in response to both antibiotic and BPNFs, while the infection in saline controls remained relatively high up to day 7 of the experiment (Figure 4b). Additionally, both BPNFs and antibiotic treatments had comparable
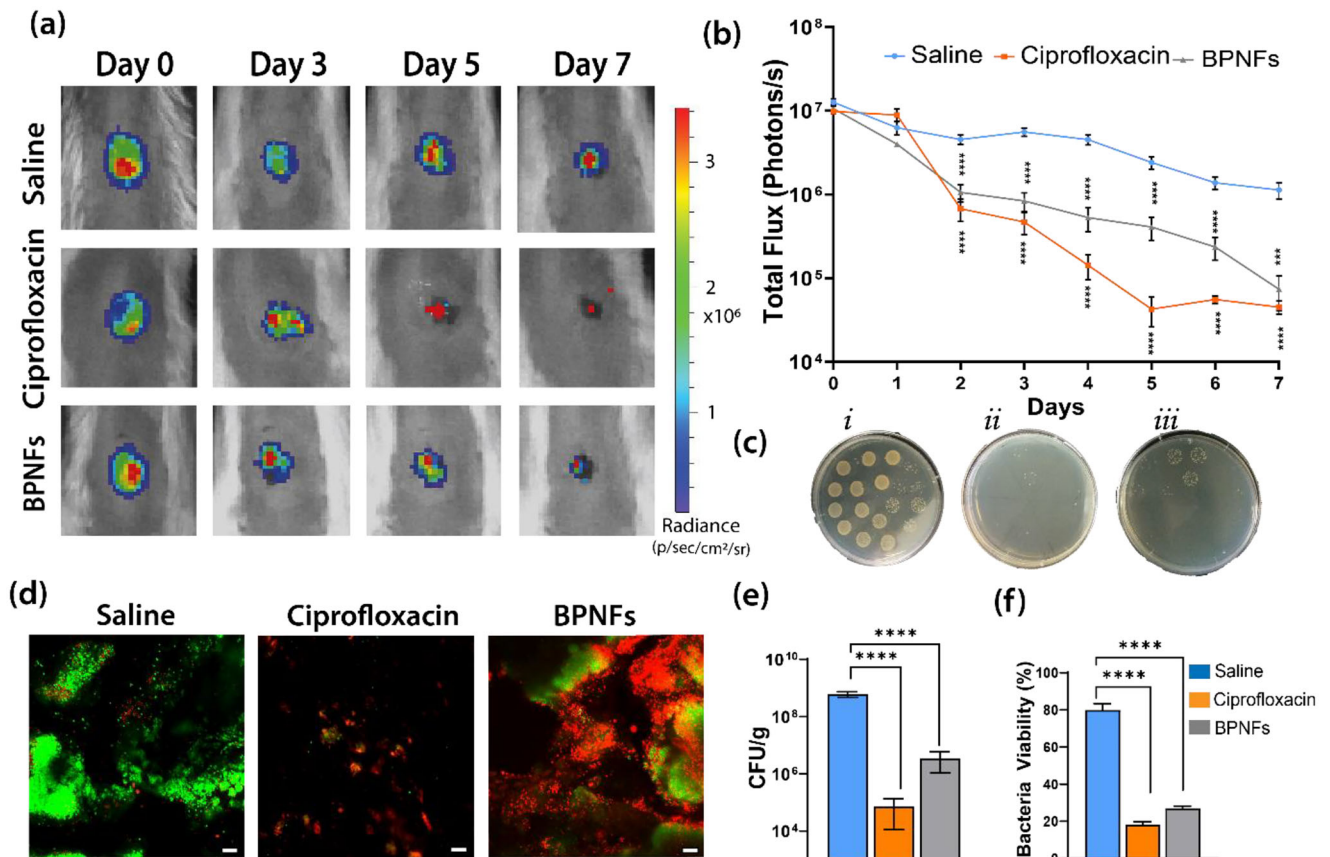
ADVANCED
SCIENCE NEWS
www.advancedsciencenews.com

ADVANCED
THERAPEUTICS
www.advtherap.com

Figure 4. BPNFs significantly reduced infection in an acutely infected mouse model over 7 days. a) Representative images of IVIS bioluminescent signal between treatment groups measured by Radiance (p/s/cm^3/r). b) Bacterial burden quantified as average total flux (Photons s^{-1}). c) Representative images of plates displaying colonies formed after treatment with i) saline, ii) ciprofloxacin iii) BPNFs. d) Representative confocal images of Live/Dead bacteria viability. e) Quantification of wound bacterial levels by assessment of colony counts (CFU g^{-1}) at day 7 post wounding. f) Quantitative analysis of average bacteria viability from confocal images (%). Scale bar 10 µm. Data are shown as mean ± SEM. *denotes a statistically significant difference, using a two-way ANOVA where **$p<0.01$ ***$p<0.001$, ****$p<0.0001$, n = 8 in each group.

effectiveness in clearing *S. aureus* infection with no significant difference noted between the two groups on day 7 using IVIS imaging (P = 0.9893) (Figure 4b). Further analysis of the *S. aureus* counts from the excised infected wounds using CFU and Live/Dead staining confirms the high level of bacterial clearance between the three treatment groups (Figure 4c,d). CFU plates show a clear decrease in the number of viable bacterial colonies for the BPNFs treatment group, compared to the saline control (Figure 4c). Importantly, BPNFs treatment resulted in an average 3 log reduction in bacterial load compared to the non-treated infected control, with no significant difference observed between the industry-standard control (ciprofloxacin antibiotic) (P = 0.9995) (Figure 4e). Lastly, analysis of bacterial cell viability using Live/Dead staining demonstrated an overall reduction in the intensity of green fluorescence in response to BP-NFs treatment compared to the saline control confirming BP-NFs ability to eradicate bacteria in wound biofilms (Figure 4d). Quantitative analysis of bacterial viability revealed 80%, 18%, and 27% bacterial viability following saline, ciprofloxacin, and BPNFs treatment respectively. Hence demonstrating similar efficacy between BPNFs and the gold standard broad-spectrum antibiotic

ciprofloxacin (Figure 4f). These results suggest that BPNFs are effective at reducing the number of viable bacteria after daily application over the 7 days. In contrast, previous in vivo studies have required external near-infrared irradiation (NIR) to initiate oxidation, promote ROS generation and therefore facilitate antimicrobial effects.[24] In those reports using thicker multi-layer BPNFs, the removal of the NIR light source resulted in incomplete bacterial destruction and therefore was deemed ineffective for treatment in vivo.[24–27,29,41] This has been demonstrated in a previous study where multi-layered Black Phosphorus demonstrated only a 33% antimicrobial efficacy without NIR compared to 77% with NIR excitation.[24]

Clinically, poor light specificity of an external laser can result in undesirable temperature rises to the surrounding wound tissue, further impairing wound healing outcomes.[40] We speculate that the combination of nanoknife effect and ROS-mediated activity of BPNFs was vital to rapidly eliminate pathogens, with sustained antibacterial effect. This unique interaction within the nano-bio interface also diminishes the opportunity for bacteria to develop resistance as also highlighted in a previous study.[42] Therefore, BPNFs offer a unique, effective, easy-to-use, and clinically

**ADVANCED
SCIENCE NEWS**

www.advancedsciencenews.com

**ADVANCED
THERAPEUTICS**

www.advtherap.com

translatable approach for the treatment of wound infections through oxidation in ambient light conditions without the need for an external light source application.

2.5. In Vivo Evaluation of Wound Healing

In the current study, BPNFs demonstrated enhanced wound healing and tissue regeneration, evident at both a macroscopic and microscopic level of analysis when compared to controls. BPNFs treatment significantly increased the healing and regeneration process, with no evidence of erythema or maceration at a macroscopic level of analysis (**Figure 5**a). An 80% wound closure over a 7-day period was observed after daily BPNFs treatment, with all quantifiable parameters suggesting that the wounds were more advanced in the regeneration process compared to the saline control or ciprofloxacin (Figure 5a,b). Interestingly, ciprofloxacin had a bigger wound area compared to saline control over the 7-day period and this is commonly observed with antibiotic-based treatments delaying wound healing responses in some instances. Furthermore, histological analysis revealed that BPNFs treatment resulted in an improvement in wound regeneration, demonstrated by a decreased wound size and degree of tissue scabbing (Figure 5d). Additionally, BPNFs improved the healing process compared to ciprofloxacin with a significant decrease in wound length ($P = 0.0381$), reduced wound gape, and an increased rate of wound re-epithelization ($P = 0.0186$) and reduced wound penniculus gape ($P = 0.0216$) (Figure 5eh). In most of these measurements, ciprofloxacin and saline control showed a similar healing profile as demonstrated by an increased wound length, gape, and decreased percentage of re-epithelization compared to the BPNFs groups. Wound re-epithelization is an important hallmark of tissue regeneration attributed to the proliferative capacity of keratinocytes into the epidermis and migration to form the new epidermis.[43,44] Therefore, the high degree of biocompatibility with skin keratinocytes and the observed improvement in the degree of re-epithelization suggests that BPNFs promote wound healing stages even when the wounds are clinically infected with a highly resistant *S. aureus* bacteria.[45]

Despite BPNFs promising antibacterial application, the wound healing properties are not well documented. No studies to date have demonstrated the healing properties of few-layered BPNFs in ambient light, however, similar effects on healing have been established in other applications of multi-layered composite-Black Phosphorus materials.[24,41] A recent study demonstrated the capacity of Black Phosphorus to act as an oxygen carrier with hemoglobin through the application of microneedles in a diabetic wound, where wound closure was evident within nine days.[41] Similarly, enhanced wound healing effects have been demonstrated following the combined application of multi-layered Black Phosphorus in conjunction with silver nanoparticles (AgNPs) and laser irradiation.[24] This study attributed the enhanced wound healing effects to the antimicrobial properties of the material. A reduced bacterial burden in a wound has been proposed to favor more rapid healing and tissue regeneration.[46] When bacteria form mature biofilms, the development of neutrophil-mediated killing resistance limits the ability of the host immune system to fight and clear infection.[46] With the assistance of an-

timicrobial therapies, including BPNFs, the reduction in localized wound infection could enable wound healing to progress past the inflammatory phase and proliferative phases and onto the final re-modeling phase of tissue repair.[47]

One possible direct mechanism of action of BPNFs could be the effect of the byproducts on tissue repair. BPNFs have previously been demonstrated to degrade into non-toxic phosphates, including phosphorous acid (H_3PO_3) and phosphoric acid (H_3PO_4).[48] The oxidation products of BPNFs are composed of 48% H_3PO_3 and 39% H_3PO_4 in water; and 77% H_3PO_3 and 23% H_3PO_4 when oxidized in the air.[48] This suggests that the oxidation of BPNFs to produce acidic byproducts could be influencing the pH of the wound microenvironment and therefore directly contributing to the enhanced healing observed in the current study. Literature suggests that the pH of the wound significantly contributes to wound healing outcomes, with an acidic wound environment favoring improved tissue healing.[49] Specifically, pH influences enzyme and fibroblast activity, keratinocyte proliferation, micro-organism growth, and immunological responses.[50] To determine whether there were any systemic effects of BPNFs or their byproducts extending to the major organs in the body, H&E staining with tissue analysis was performed. No toxicity, inflammation, tissue necrosis, or BPNFs deposits were observed in the heart, kidney, liver, lung, or spleen (**Figure 6**). This suggests that few-layered BPNFs were highly biocompatible for use in the treatment of wound infections; consistent with previous in vivo applications demonstrating the safety of BPNFs.[24,26–28]

2.6. Inflammatory Response of BPNFs

Quantification of neutrophils and macrophage phenotype in the wound bed was performed to determine the influence of treatments on the local inflammatory response of locally infected wounds. Analysis of NIMP-R14 positive neutrophils showed that the BPNFs treatment resulted in a significant decrease in the number of neutrophils in the wound bed (**Figure 7**a). Quantitative analysis revealed an average 40% decrease in the number of neutrophils compared to the saline control on day 7 of the trial ($P = 0.0121$) (Figure 7b). While antibiotic treatment also had a trend toward reduced neutrophil infiltration into the wound bed this was not significantly different to either saline control. Infiltration of neutrophils into the wound bed is normally observed during the inflammatory phase to clear micro-organism infection and other cellular debris and is required for healing and host responses to localized wound infection.[21,51] However, the continual recruitment of neutrophils can prolong inflammation and result in the formation of chronic non-healing wounds that do not progress past the inflammatory stage.[51] Current findings suggest that a decrease in neutrophils observed following BPNFs treatment could favor the progression of healing from the inflammatory phase to the proliferative phase and the final remodeling phase suggesting that these wounds have progressed further along the healing pathway. This is in agreement with a previous study that described similar effects on wounds from treatment with composite-Black Phosphorus materials where significantly fewer inflammatory cells were observed in a diabetic wound when Black Phosphorus was delivered in a gel and irradiated with
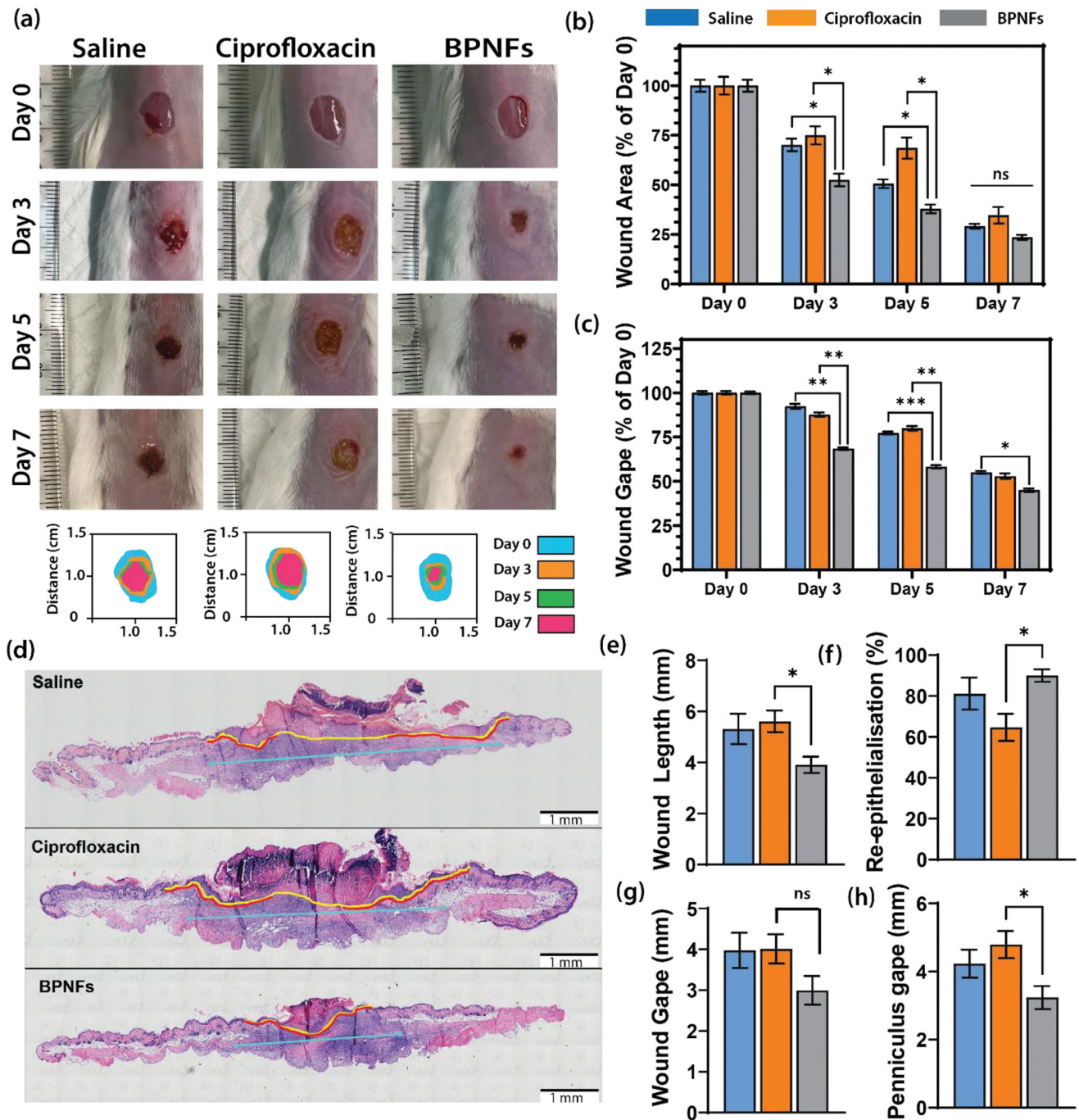
ADVANCED
SCIENCE NEWS

www.advancedsciencenews.com

ADVANCED
THERAPEUTICS

www.advtherap.com

Figure 5. BPNFs enhance the healing rate of infected mice wounds over a 7-day period. a) Representative digital photographs and schematic traced wounds demonstrating the rate of healing and wound closure. b,c) Wound area and wound gape measured as a % of day 0. d) Representative images of H&E-stained wounds for each treatment group. The yellow line denotes wound length, the blue arrow denotes wound gape, and the red line denotes wound re-epithelization (%). eh) Quantitative analysis of wound parameters including wound length (mm), wound re-epithelization (%), wound gape (mm), and panniculus gape (mm). Data are shown as mean ± SEM. * denotes significance between groups using a two-way ANOVA where *$p<0.05$, **$p<0.01$, ***$p<0.001$, n = 10 in each group. Scale bar 1 mm.

NIR light.[29] The study attributed the low number of neutrophils to the excellent bacterial clearance of the material.

Wound inflammation was further analyzed using macrophage phenotype. The macrophage infiltration and phenotype using markers of M1 (F4/80+ (green)) and M2 (F4/80+/YM-1+ (orange)) demonstrated distinct differences between the treatment groups (**Figure 8**a). Notably, M2 anti-inflammatory macrophage expressing both F4/80/YM-1 was higher for the ciprofloxacin and BPNFs. The ratio of the macrophage phenotype showed a significantly higher M2/M1 ratio in BPNFs-and
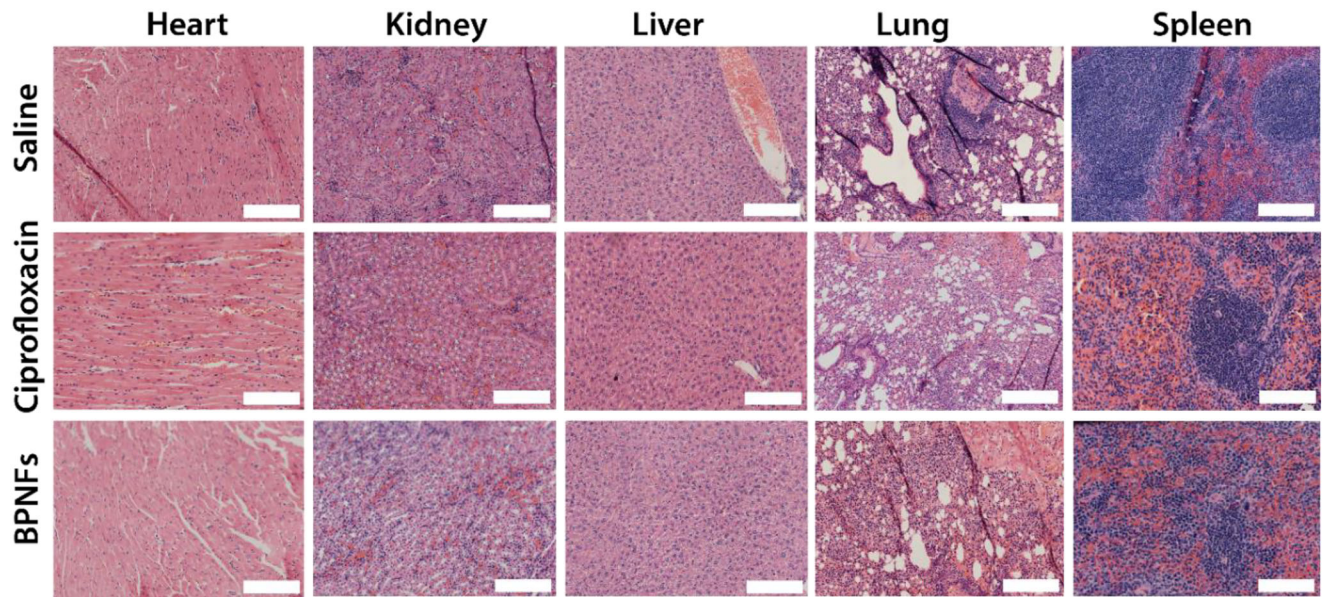
Figure 6. Treatment with BPNFs did not result in any tissue inflammation, toxicity, or necrosis in the major organs of mice. Histological sections (H&E stained) from five major organs of mice at 7 days post-wounding, including heart, kidney, liver, lung, and spleen. Scale bar 200 μm.

ciprofloxacin-treated wounds compared to saline control however this was not significant for the antibiotic-treated group (Figure 8a,b). These measurements are consistent with the neutrophil analysis showing reduced neutrophils in the wound area suggesting resolved wound inflammation. Therefore, there is a strong indication that BPNFs help to significantly reduce wound inflammation by controlling neutrophil and macrophage populations within the wound bed to facilitate both infection clearance and progression of the healing process. This also attributes to improved wound healing outcomes observed. The current study

now highlights the role of BPNFs in clearing infection and promoting wound healing in ambient light as indicated by accelerated wound closure, re-epithelization, and controlled wound inflammation.

3. Conclusion

In conclusion, the current study demonstrated that novel BPNFs can be developed to maintain a high degree of stability and biological activity serving as a promising antibacterial agent for wound
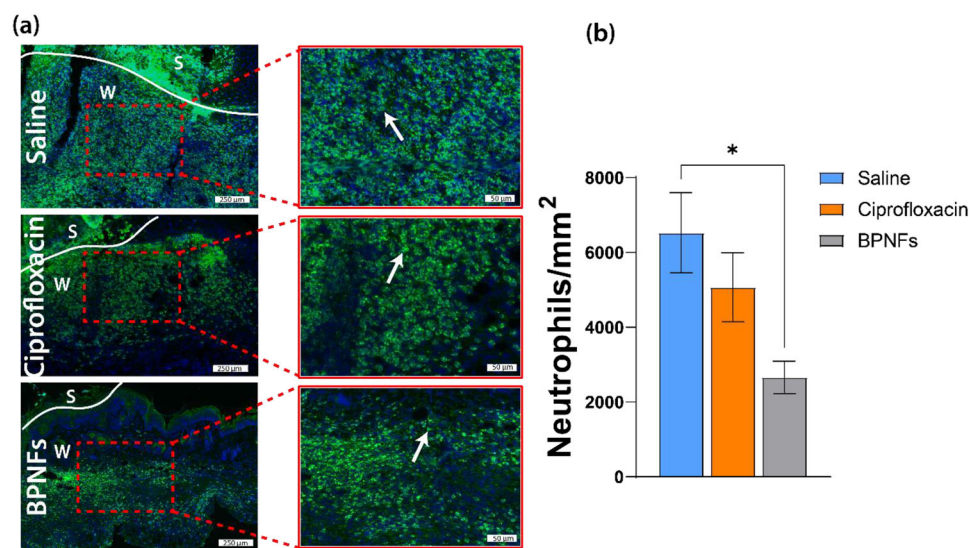

Figure 7. BPNFs decreased the number of neutrophils present in the wound bed on day 7. a) Representative images of the stained neutrophils in the wound bed for the three treatment groups. "S" denotes scab region and "W" denotes wound bed. White arrows indicate the multilobulated nucleus of neutrophil cells. b) Quantification of wound inflammation in *S. aureus* infected wounds by analysis of NIMP-R14+ve neutrophil cells in wounds of mice treated with BPNFs, antibiotic or saline control. Data are shown as mean ± SEM. * denotes significance using a one-way ANOVA where $^*p < 0.05$, n = 5 in each group. Scale bar 250 and 50 μm for the magnified images.

2300235 (10 of 14)

**ADVANCED
SCIENCE NEWS**

www.advancedsciencenews.com
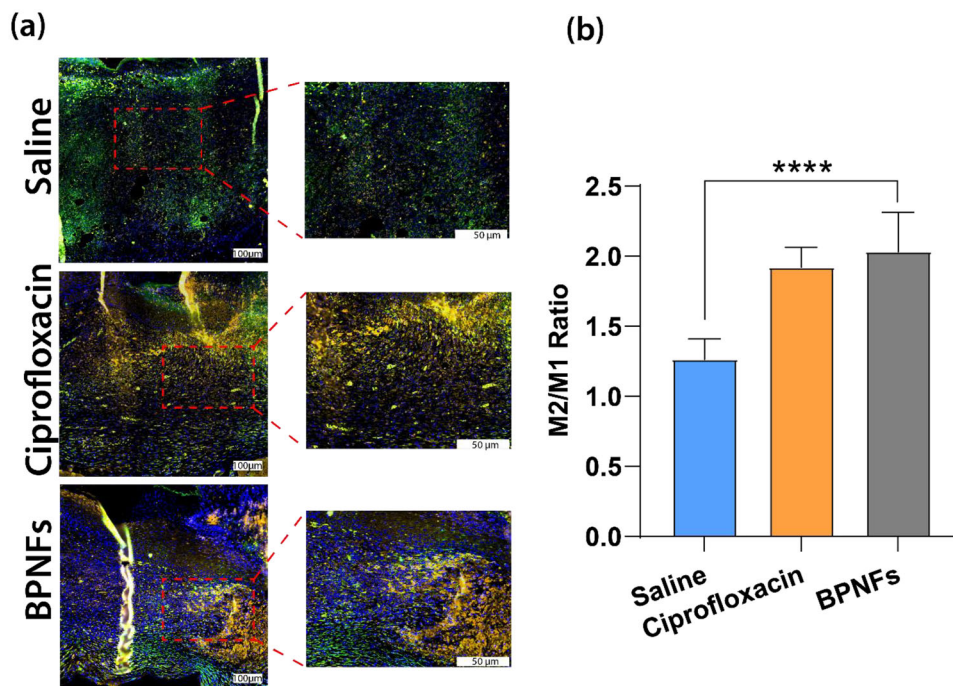
**ADVANCED
THERAPEUTICS**

www.advtherap.com

Figure 8. BPNFs increase anti-inflammatory macrophage. a) Representative images of immunofluorescent macrophages by F4/80 (green) and YM-1 (orange) staining counterstained with DAPI (blue) in wounds. b) The ratio of M2/M1 macrophage phenotype in wound bed of saline control, ciprofloxacin, and BPNFs treatment. Data are shown as mean ±SEM and the * denotes a significant difference compared to saline control ($p < 0.05$) using one-way ANOVA followed by Dunnett's multiple comparison test. ****$p < 0.0001$. Scale bar 100 and 50 μm.

management applications. Importantly, when BPNFs were exfoliated into a "few-layer" structure, the oxidation properties in ambient light increased in vitro antibacterial effects against both gram-positive and gram-negative pathogens, with negligible toxicity toward mammalian skin cells. We demonstrate that BPNFs are also highly effective against in vivo wound infection by demonstrating successful reduction of *S. aureus* infection following daily topical application over a 7-day period. This demonstrates that few-layered BPNFs can elicit in vivo antimicrobial effects through oxidation in ambient conditions, without the assistance of NIR light activation, enabling broader application of this material in clinical wound management. Importantly, BPNFs had a significantly positive impact on healing demonstrated by accelerated and enhanced wound closure, increased re-epithelization, and reduced inflammatory responses, all contributing to favorable tissue regeneration. These results provide an opportunity to progress a few-layered BPNFs along the commercialization pathway toward a novel, effective management option for the treatment of wounds infected with antibiotic-resistant bacteria.

4. Experimental Section

Preparation and Exfoliation of BPNFs: The BPNFs were prepared using liquid-phase exfoliation similar to the previously reported approach.[19,34] The bulk Black Phosphorus crystal (130 mg) was mechanically ground into a powder and resuspended in 20 mL of dimethyl sulfoxide (DMSO). The Black Phosphorus suspension was then exfoliated using a probe ultrasonicator (ScientZ-IID) for 6 h (130 W). Before characterization, the BPNF solution was twofold serial diluted in DMSO and drop cast onto the relevant surface. The surfaces were then dried on a hotplate, then further

dried under the flow of N_2 gas to remove any excess DMSO.[52] The samples were then stored under vacuum for future experiments. For biological applications, the BPNF solution was purified through a series of washing processes with milliQ water to remove the excess DMSO and finally resuspended in milliQ water at the desired concentration. As Black Phosphorus was light sensitive, all samples were prepared and stored under dark conditions.

BPNFs Characterization: The solution of BPNFs was characterized through a series of chemical and physical assessments using established protocols.[19,34] A Horiba LabRAM HR Evolution Micro-Raman system equipped with a 532 nm laser source (50× objective) was used to obtain the Raman spectra for the BPNFs. Scanning electron micrographs of the BPNFs were obtained using a FEI Verios field-emission gun scanning electron microscope (VP, Oberkochen, BW, Germany). Micrographs were obtained using 3 kV. EDS maps of BPNFs were obtained using an Oxford XMax30 EDX Detector using 15 kV. TEM A JEOL JEM-2100F TEM equipped with a field emission gun operating at 200 kV was used to image the BPNFs. The TEM instrument was equipped with a Gatan OneView 4k camera. AFM images were obtained using a Cypher ES AFM (Oxford Instrument, Asylum Research, Santa Barbara, CA, USA). All AFM measurements were taken using AC240 cantilevers (Oxford Instrument, Asylum Research, Santa Barbara, CA, USA, nominal spring constant $k_c = 2 \text{ N m}^{-1}$) which were tuned using the thermal spectrum method. The AFM was operated in AC mode using a set point ratio (Imaging Amplitude (A)/free amplitude (A0)) of >0.7 to minimize imaging forces. The resulting height profiles of the BPNFs were processed using Gwyddion.

Mammalian Cell Cytotoxicity: Human Keratinocytes (HaCaTs) and Human Foreskin Fibroblast cells (HFFs) were grown in Dulbecco's Modified Eagle's Medium (DMEM) (ThermoFisher Scientific, Australia) (supplemented with 20% Fetal Calf Serum (FCS), 1% PenicillinStreptomycin (PS) at 37°C, 5% CO_2. Cells were exposed to a twofold serial dilution of stock solution of BPNFs (10 mg mL^{-1}) and further incubated for 24 h. The cells were stained with 10% Resazurin solution (ThermoFisher Scientific, Australia) and incubated for 2 h at 37°C. Fluorescence (540 nm/590 nm) was

measured using the FLUOstar Optima Microplate reader (BMG Lab Tech, UK, 2022) using standard protocols.[53]

Live/Dead Mammalian Cell Viability: Cell viability was quantified using the Live/Dead Viability/Cytotoxicity Kit for mammalian cells (ThermoFisher Scientific, Australia) following manufacturer's recommendations and previously published studies.[53] Human Foreskin Fibroblasts and Human Keratinocytes were grown to 95% confluency on glass coverslips in a 24-well plate. Cells were stained with a combination of 2 μL of calcein AM (component A) and 8 μL of ethidium homodimer-1 (component B) combined with 4 mL of PBS. 200 μL was dispensed into each well and incubated at room temperature (2025°C) for 30 min. Cells were imaged using an Olympus IX81 light microscope (Olympus, Tokyo, Japan) using channels 494/517 nm (for component A) and 528/617 nm (for component B). Cell viability was quantified using the software ImageJ (NIH, Bethesda, MD, America) following established protocols.[53]

In Vitro Antibacterial Assessments: *Minimum Inhibitory Concentration (MIC)*-The minimum inhibitory concertation (MIC) was determined using the microdilution method according to the previous protocols.[54] *S. aureus* (ATCC12600) (Xen 29) (Perkin Elmer, UK), *S. aureus (ATCC 19606 (MRSA), Pseudomonas aeruginosa (PAO1), S. epidermidis* (ATCC 35984) and *Escherichia coli* (10P50) were sourced from frozen stock at −80°C and grown on a tryptic soya agar (TSA). The *S. aureus* Xen 29 were grown on a selective TSA plate supplemented with 200 μg mL^{-1} kanamycin. The overnight culture was grown by suspending a single colony into a selective tryptic soya broth (TSB) medium and incubated at 37°C for 24 h. Briefly, TSB and respective treatment at equal volumes were mixed using 96-well plates. The treatments included the following: a twofold concentration of BPNFs and controls, PBS, antibiotic kanamycin, growth control, and sterility control. Bacteria (10 μL) was dispensed into each of the wells at a final concentration of 5×10^5 CFU mL^{-1} and returned to the incubator for 24 h. The MIC was measured using a microplate reader or quantified using the Xenogen IVIS Spectrum Imaging system (Caliper Life Sciences, Massachusetts, America).

Time-Dependent Antibacterial Effect-The bacterial viability was quantitatively evaluated using the Live/Dead Baclight viability kit as per the manufacturer's manual (Invitrogen, Thermo Fisher Scientific). An overnight culture of *S. aureus* and *P. aeruginosa* was cultured in TSB at 37°C and then diluted to 1×10^6 CFU mL^{-1}. Aliquots of the bacterial suspension were grown on a sterile glass coverslip and treated with BPNFs and the negative control after 2, 6, and 24 h of exposure. Then, the bacterial cells were stained with SYTO9 and propidium iodide. The samples were incubated in the dark for 15 min at 25°C, followed by a PBS wash. The glass coverslips were mounted on a microscope slide to be imaged via an Olympus FV3000 confocal laser scanning microscope. The number of live and dead cells was quantified using ImageJ software (Fiji) 1.52a.

Animal Ethics: All experimental procedures and protocols were approved by the University of South Australia Animal Ethics Committee (U03-22). All procedures abided by the Animal Welfare Act and the Principles of the Australian Code for the care and use of animals for scientific purposes.

Excisional Murine Acute Wound Infection Model: A well-developed preclinical model of *S. aureus* acute wound infection was used in this study as previously described.[55] Briefly, on day 0, mice were administered a pre-operative analgesic buprenorphine (0.1 mg kg^{-1}) 60 μL in 0.9% saline subcutaneously 30 min prior to surgery. The animals were anesthetized through inhalation of 2.5% isoflurane gas and 2/L O_2 in a sealed chamber. The fur was removed with hair removal cream (Veet) for 1 min after which the skin was sterilized with a betadine and 70% alcohol wash. An excisional wound was created on the dorsal side of the animal using a 6 mm punch biopsy (Acu-Punch, Australia). Digital images of the wounds were taken daily for macroscopic analysis of wound healing. Mice wounds were inoculated with 10 μL of *S. aureus* bacteria 3 h post-wounding and were baseline imaged using the Xenogen IVIS Spectrum Imaging system to ensure equal wound inoculation of 5×10^6 CFU. The total photon emission from the region of interest (ROI) within the defined wound area was quantified using living ImageR software (Perkin Elmer, UK). Wounds were treated daily with topical application of 30 μL of the respective treatment (BPNFs solution, saline control, or antibiotic ciprofloxacin control) and

imaged using Xenogen IVIS Spectrum Imaging system to enable quantification of bacterial load and treatment efficacy. The BPNFs concentration used for in vivo studies was determined from the MIC assay. The highest dose of BPNFs (1500 μg mL^{-1}) was applied in 30 μL equivalent to 45 μg BPNFs per mouse wound. On day 7, the mice were humanely killed using CO_2 asphyxiation and cervical dislocation. Wounds were excised, half of the wound was processed for histology, a quarter for CFUs analysis, and a quarter for analysis of biofilm biomass. Organs including the liver, kidney, spleen, heart, and lung were removed from three mice from each group. All collected tissues were placed into cassettes and fixed in 10% formalin for 24 h, before being transferred to 70% ethanol the following day for tissue processing and histology following established protocols.[56]

Macroscopic and Microscopic Analysis of Wound healing: For macroscopic assessment of wound healing, daily digital images of wounds were analyzed using ImageProPlus (Media Cybernetics, Inc., Bethesda, MD, America). Macroscopic analysis of wound area wound gape and microscopic histological analysis of wound length, dermal gape, panniculus gape, and wound re-epithelization were performed using previously established protocols.[57] Wound tissue and major organs were processed, paraffin-embedded, and cut into 4 μm thickness using a Microtome (Leica Biosystems, Victoria, Australia). The sections were stained for hematoxylin and eosin (H&E) using previously established protocols.[58] Images were taken using an Olympus IX81 light microscope (Olympus, Tokyo, Japan) and ImageProPlus program used in wound healing analysis. Sections of major organs were examined for microscopic particles or deposits of BPNFs and any pathological changes or tissue inflammation.

Assessment of Wound Inflammation: Collected tissue samples were also immuno-stained for inflammatory markers within the wound bed using the previously described protocols.[58] Sections were deparaffinized and subjected to antigen retrieval solution (TRS) in an Antigen Decloaker (Biocare, Medical, USA) at 90°C for 10 min followed by a PBS wash and enzymatic digestion using 0.0625 g of Trypisin (SigmaAldrich, Sydney, Australia) dissolved in PBS and pre-warmed to 37°C. The sections were washed in PBS and blocked using 3% blocking serum NGS for 45 min, followed by a primary antibody NIMP-R14, Rat Monoclonal Antibody (0.5 μg mL^{-1}, sc-59338, Santa Cruz Biotechnology, Dallas, TX, USA) F4-80 Rat anti (0.5 μg mL^{-1}, MCA497R Bio-Rad Laboratories) and YM-1 Rabbit anti (0.37 μg mL^{-1}, 60130 Stem Cell Technologies) in a blocking buffer (3% NGS in PBS) overnight at 4°C. Sections were washed for 2 min in PBS three times and then incubated with Alexa Fluor 488, Goat-anti-Rat IgG (5 μg mL^{-1}, Invitrogen, CA, USA) for 1 h in the dark at room temperature. Nuclei were stained with 4',6-diamidino-2-phenylindole (DAPI) (Sigma Aldrich) at a 1:5000 dilution of 1 mg mL^{-1} stock. Slides were washed three times for 2 min in PBS to remove any unspecific binding and mounted using a fluorescence medium (DAKO Corporation, Australia). Slides were stored at −20°C and wound sections were imaged using an Olympus IX81 epifluorescence microscope (Olympus, Tokyo, Japan). Assessment of neutrophil and macrophage infiltration into the wound bed was analyzed using CellSens Imaging Software (Olympus, Tokyo, Japan) quantified as fluorescence intensity per area. Negative controls were included to demonstrate antibody staining specificity. All control sections had negligible immunofluorescence.

In Vivo Antibacterial Assessments: *Colony Forming Units (CFU)*-CFU counts were completed using infected wounds from day 7 of the mouse experiment to verify the number of viable *S. aureus* bacteria in the wounds and confirm infection quantification obtained by using IVIS bioluminescent imaging. Using the spot plate method under sterile conditions, one-quarter of the tissue sample was resuspended in sterile PBS and homogenized by vortexing three times and a further 2-min sonication. Homogenates were further serially diluted in PBS (1:20 dilution) in a 96-well plate and 20 μL spots for each dilution were dispensed in triplicate onto selective TSA plates. After allowing the spots to completely dry for 5 min, the plates were moved to a 37°C incubator. After overnight incubation, visible colonies were counted manually.

Bacterial Viability (Live/Dead Tissue Staining)-Bacterial viability was evaluated using a Live/Dead Baclight viability kit (Invitrogen, Thermo Fisher Scientific, Australia). Wound tissue was washed using PBS and then stained using a 1:1 ratio of 3 μL mL^{-1} of STYO9 (live cell stain) and with

**ADVANCED
SCIENCE NEWS**

www.advancedsciencenews.com

**ADVANCED
THERAPEUTICS**

www.advtherap.com

Propidium Iodide (dead cell stain) in PBS. The STYO9 dye binds to nucleic acids of intact cells, allowing it to fluoresce green under a 485 nm wavelength laser. The Propidium Iodide binds to the nucleic acids of dead cells and fluoresces red under a 561 nm wavelength laser. After staining for 20 min in the dark, the tissue was placed on a glass coverslip and mounted on a microscope glass slide. Images were taken using the Olympus FV3000 Confocal Laser Scanning Microscopy. Bacterial viability was quantified using ImageJ software following previously established protocols.[13]

Statistical Analysis: Statistical analyses were performed using GraphPad Prism version 8.0 (GraphPad, Sacramento, California, America). Data were analyzed with a one-way ANOVA or two-way ANOVA. *Post hoc* comparisons were completed using a Tukey *post hoc* test to see if significance was present. Significance was denoted at $p < 0.05$ and all data presented as mean $\pm$ standard error of the mean (SEM) unless otherwise noted.

Supporting Information

Supporting Information is available from the Wiley Online Library or from the author.

Conflict of Interest

The authors declare no conflict of interest.

Author Contributions

E.P.V. and H.H. contributed equally to this work. The manuscript was written through the contribution of all authors. All authors have approved the final version of the manuscript.

Data Availability Statement

The data that support the findings of this study are available from the corresponding author upon reasonable request.

[1] A. Hayes, J. Satiaputra, L. Sternicki, A. Paparella, Z. Feng, K. Lee, B. Blanco-Rodriguez, W. Tieu, B. Eijkelkamp, K. Shearwin, T. Pukala, A. Abell, G. Booker, S. Polyak, *Antibiotics* **2020**, *9*, 165.

[2] O'Neill, The Review of Antimicrobial Resistance: Tackling drug resistant infections globally, UK Goverment, **2014**. https://amr-review.org/sites/default/files/AMR%20Review%20Paper%20-%20Tackling%20a%20crisis%20for%20the%20health%20and%20wealth%20of%20nations_1.pdf

[3] I. Negut, V. Grumezescu, A. Grumezescu, *Molecules* **2018**, *23*, 2392.

[4] S. Roy, S. Santra, A. Das, S. Dixith, M. Sinha, S. Ghatak, B. Blackstone, H. Powell, V. Bergdall, D. Wozniak, C. Sen, *Ann. Surg.* **2020**, *271*, 1174.

[5] C. Lux, *Vet. Dermatol.* **2022**, *33*, 91.

[6] P. Filius, I. Gyssens, *Am. J. Clin. Dermatol.* **2002**, *3*, 1.

[7] R. Chang, S. Morales, Y. Okamoto, H.-K. Chan, *J. Lab. Clin. Med.* **2020**, *220*, 153.

[8] B. Lipsky, M. Dryden, F. Gottrup, D. Nathwani, R. Seaton, J. Stryja, *J. Antimicrob. Chemother.* **2020**, *13*, 13.

[9] A. Pinto, M. Cerqueira, M. Bañobre-Lópes, L. Pastrana, S. Sillankorva, *Viruses* **2020**, *12*, 235.

[10] H. Haidari, S. Garg, K. Vasiliev, Z. Kopecki, A. Cowin, *J. Wound Pract. Res.* **2020**, *28*, 173.

[11] V. Dalal, S. Biswas, in *Functional Bionanomaterials: From Biomolecules to Nanoparticles*, Springer, Cham, Switzerland **2020**.

[12] J. Ouyang, C. Feng, X. Zhang, N. Kong, W. Tao, *Acc. Mater. Res.* **2021**, *2*, 489.

[13] H. Haidari, Z. Kopecki, R. Bright, A. Cowin, S. Garg, N. Goswami, K. Vasilev, *ACS Appl. Mater. Interfaces* **2020**, *12*, 41011.

[14] H. Haidari, K. Vasilev, A. Cowin, Z. Kopecki, *ACS Appl. Mater. Interfaces* **2022**, *14*, 51744.

[15] C. Beer, R. Foldbjerg, Y. Hayashi, D. Sutherland, H. Autrup, *Toxicol. Lett.* **2012**, *208*, 286.

[16] A. Oliveira, S. Simões, A. Ascenso, C. Reis, *J. Dermatol.* **2022**, *33*, 2.

[17] Y. Abate, D. Akinwande, S. Gamage, H. Wang, M. Snure, N. Poudel, S. Cronin, *Adv. Mater.* **2018**, *30*, 1704749.

[18] C. Zhang, Y. Wang, J. Ma, Q. Zhang, F. Wang, X. Liu, T. Xia, *Sci. Total Environ.* **2020**, *721*, 137740.

[19] Z. Shaw, S. Cheeseman, L. Huang, R. Penman, T. Ahmed, S. Bryant, G. Bryant, A. Christofferson, R. Orrell-Trigg, C. Dekiwadia, V. Truong, J. Vongsvivut, S. Walia, A. Elbourne, *J. Mater. Chem. B* **2022**, *10*, 7527.

[20] S. Walia, S. Balendhran, T. Ahmed, M. Singh, C. El-Badawi, M. Brennan, P. Weerathunge, N. Karim, F. Rahman, A. Rassell, J. Duckworth, R. Ramanathan, G. Collis, C. Lobo, M. Toth, J. Kotsakidis, B. Weber, M. Fuhrer, J. Dominguez-Vera, M. Spencer, I. Aharonovich, S. Sriram, M. Bhaskaran, V. Bansal, *Adv. Mater.* **2017**, *29*, 1700152.

[21] T. Guo, S. Zhuang, H. Qiu, Y. Guo, L. Wang, G. Jin, W. Lin, G. Huang, H. Yang, *Part. Part. Syst. Charact.* **2020**, *37*, 2000169.

[22] Z. Shaw, S. Kuriakose, S. Cheeseman, E. Mayes, A. Murali, Z. Oo, T. Ahmed, N. Tran, K. Boyce, J. Chapman, C. McConville, R. Crawford, P. Taylor, A. Christofferson, V. Truong, M. Spencer, A. Elbourne, S. Walia, *ACS Appl. Mater. Interfaces* **2021**, *13*, 17340.

[23] Q. Zhou, Q. Chen, Y. Tong, J. Wang, *Angew. Chem., Int. Ed. Engl.* **2016**, *55*, 11437.

[24] M. Liang, M. Zhang, S. Yu, Q. Wu, K. Ma, Y. Chen, X. Liu, C. Li, F. Wang, *Small* **2020**, *16*, 1905938.

[25] P. Ran, W. Chen, H. Zheng, J. Zhou, B. Qiu, W. Cao, X. Li, *Nanoscale* **2021**, *13*, 13506.

[26] X.-W. Huang, J.-J. Wei, M.-Y. Zhang, X.-L. Zhang, X.-F. Yin, C.-H. Lu, H.-H. Yang, *ACS Appl. Mater. Interfaces* **2018**, *10*, 35495.

[27] S. Huang, S. Xu, Y. Hu, X. Zhao, L. Chang, Z. Chen, X. Mei, *Acta Biomater.* **2022**, *137*, 199.

[28] J. Ouyang, R.-Y. Liu, W. Chen, Z. Liu, Q. Xu, K. Zeng, L. Deng, L. Shen, Y.-N. Liu, *J. Mater. Chem. B* **2018**, *6*, 6302.

[29] J. Ouyang, X. Ji, X. Zhang, C. Feng, Z. Tang, N. Kong, A. Xie, J. Wang, X. Sui, L. Deng, Y.-N. Liu, J. Kim, Y. Cao, W. Tao, *Proc. Natl. Acad. Sci.* **2020**, *117*, 28667.

[30] A. Naskar, S. Lee, K. Kim, *Pharmaceutics* **2021**, *13*, 52.

[31] S. Bose, D. Surendhiran, B.-S. Chun, S. Arthanari, V. Tran, H. Lee, H. Kang, *Colloids Surf., B* **2022**, *219*, 112807.

[32] H. Zheng, H. Li, H. Deng, W. Fang, X. Huang, J. Qiao, Y. Tong, *Colloids Surf., B* **2022**, *214*, 112433.

[33] G. Qu, T. Xia, W. Zhou, X. Zhang, H. Zhang, L. Hu, J. Shi, X. Yu, G. Jiang, *Chem. Rev.* **2020**, *120*, 2288.

[34] Z. Sun, Y. Zhang, H. Yu, C. Yan, Y. Liu, S. Hong, H. Tao, A. Robertson, Z. Wang, A. Pádua, *Nanoscale* **2018**, *10*, 12543.

[35] S. Kuriakose, T. Ahmed, S. Balendhran, G. Collis, V. Bansal, I. Aharonovich, S. Sriram, M. Bhaskaran, S. Walia, *Appl. Mater. Today* **2018**, *12*, 244.

[36] A. Łapińska, A. Taube, J. Judek, M. Zdrojek, *J. Phys. Chem.* **2016**, *120*, 5265.

[37] T. Ahmed, S. Kuriakose, S. Abbas, M. Spencer, M. Rahman, M. Tahir, Y. Lu, P. Sonar, V. Bansal, M. Bhaskaran, S. Sriram, S. Walia, *Adv. Funct. Mater.* **2019**, *29*, 1901991.

[38] T. Ahmed, S. Kuriakose, E. Mayes, R. Ramanathan, V. Bansal, M. Bhaskaran, S. Sriram, S. Walia, *Small* **2019**, *15*, 1900966.

[39] X. Ding, Z. Wei, Y. Chen, P. Lin, Q. Yan, Y. Fan, X. Chen, Z. Cheng, *Opt. Mater. Express* **2019**, *9*, 423.

[40] J. Zhang, Y. Cao, C. Chen, Q. Wang, Y. Shao, *Phys. Status Solidi B* **2022**, *259*, 2100543.

[41] X. Zhang, G. Chen, Y. Liu, L. Sun, L. Sun, Y. Zhao, *ACS Nano* **2020**, *14*, 5901.

[42] H. Haidari, R. Bright, Z. Kopecki, P. Zilm, S. Garg, A. Cowin, K. Vasilev, N. Goswami, *ACS Appl. Mater. Interfaces* **2022**, *14*, 390.

[43] S. Guo, L. DiPietro, *J. Dent. Res.* **2010**, *89*, 219.

[44] H. Haidari, R. Bright, X. Strudwick, S. Garg, K. Vasilev, A. Cowin, Z. Kopecki, *Acta Biomater.* **2021**, *128*, 420.

[45] J. Domizio, C. Belkhodja, P. Chenuet, A. Fries, T. Murray, P. Mondéjar, O. Demaria, C. Conrad, B. Homey, S. Werner, D. Speiser, B. Ryffel, M. Gilliet, *Nat. Immunol.* **2020**, *21*, 1034.

[46] J. Hirschfeld, *J. Oral. Microbiol.* **2014**, *6*, 26102.

[47] P. Bowler, B. Duerden, D. Armstrong, *Clin. Microbiol. Rev.* **2001**, *14*, 244.

[48] J. Plutnar, Z. Sofer, M. Pumera, *ACS Nano* **2018**, *12*, 8390.

[49] E. Jones, C. Cochrane, S. Percival, *Adv. Wound Care* **2015**, *4*, 431.

[50] S. Percival, S. McCarty, J. Hunt, E. Woods, *Wound Repair Regen.* **2014**, *22*, 174.

[51] T. Wilgus, S. Roy, J. McDaniel, *Adv. Wound Care* **2013**, *2*, 379.

[52] P. Yasaei, B. Kumar, T. Foroozan, C. Wang, M. Asadi, D. Tuschel, J. Indacochea, R. Klie, A. Salehi-Khojin, *Adv. Mater.* **2015**, *27*, 1887.

[53] H. Haidari, Z. Kopecki, A. Sutton, S. Garg, A. Cowin, K. Vasilev, *Antibiotics* **2021**, *10*, 49.

[54] H. Haidari, N. Goswami, R. Bright, Z. Kopecki, A. Cowin, S. Garg, K. Vasilev, *Nanoscale Adv.* **2019**, *1*, 2365.

[55] H. Haidari, R. Bright, X. L. Strudwick, S. Garg, K. Vasilev, A. J. Cowin, Z. Kopecki, *Acta Biomater.* **2021**, *128*, 420.

[56] J. Jackson, Z. Kopecki, A. Cowin, *J. Nanomater.* **2013**, *2013*, 1.

[57] Z. Kopecki, N. Stevens, G. Yang, E. Melville, A. Cowin, *Int. J. Mol. Sci.* **2018**, *19*, 2014.

[58] H. Haidari, R. Bright, S. Garg, K. Vasilev, A. Cowin, Z. Kopecki, *Biomedicines* **2021**, *9*, 1182.

2300235 (14 of 14)